Electron-detachment cross sections for $O^- + N_2$ near the free-collision-model velocity threshold

A. A. Martínez-Calderón [1], M. M. Sant'Anna [2], and G. Hinojosa [1,*]

[1]*Instituto de Ciencias Físicas, Universidad Nacional Autónoma de México, Apartado Postal 48-3, Cuernavaca 62251, Mexico*
[2]*Instituto de Física, Universidade Federal do Rio de Janeiro, Caixa Postal 68528, Rio de Janeiro 21941-972, RJ, Brazil*

We present measurements of the total projectile-electron-loss cross sections in $O^- + N_2$ collisions in the energy range from 2.5 to 8.5 keV. Two different techniques, beam attenuation and the growth rate, are employed. The cross sections measured using the growth-rate method show a threshold behavior. We analyze the cross-section velocity dependence in the framework of a collision between a quasifree electron, loosely bound to the projectile, and the molecular target. Within the free-collision model, we deduce and test a simple analytical expression for the expected velocity threshold taking into account the angular distribution of electron velocities within the anion.

I. INTRODUCTION

In negative ions, the extra electron is bound to its neutral core by weak Coulomb-screened potentials and by electron correlation effects. For this reason, both structure and collision models, even for the simplest cases, demand highly electronically correlated approaches and are, in turn, a severe testbed for state-of-the-art theoretical methods. Such may be the case of the formation of negative methane [1] and the extremely long-lived CCH_2^- anion [2].

Negative ions are, in general, an important species in Nature. Their presence in cold plasmas [3,4] is relevant to the electronic density function since they are a source of thermal electrons. In atmospheric environments, anions were found in the upper atmosphere of Titan satellite [5], and in the coma of comets [6], and are of importance in artificial atmosphere generation [7]. In the case of the interstellar medium (IM) [8], despite the hostile conditions for their permanence, negative ions are abundant and a well-established fact. Understanding their presence in the IM constitutes a current question in science [9]. Even in the well-established field of small-mass spectrometry, a new molecular ion species CH_4^- (of $M/q = -16$) has been reported [1,10]. Particularities of negative-ion projectiles, when compared to the more simple positive-ion or atomic projectiles, are observed in the search for more general scaling laws for projectile-electron-loss cross sections [11–16]. Due to strong correlation effects, the comparison of different anions belonging to the same line of the periodic table shows no evident regularity, which results in difficulty to find simple scaling laws for collisions involving anionic projectiles. These questions prompt the need for more fundamental studies about this kind of ions and their interactions.

Even for a projectile as simple as an electron, scattering by the N_2 target shows a large variety of involved processes [17]. When the projectile has internal structure, and the high degree of electronic correlation characteristic to anions, the complexity of the collision system increases significantly. In this paper, we present measurements of electron-detachment cross sections for the $O^- + N_2$ collision system. The measurements reproduce the discrepancy between the two techniques which is a question at the low-energy interval for a number of collision systems.

The velocity range of the cross sections reported here allows a study of the onset of a projectile-electron-loss mechanism with a quasifree-electron behavior. The experimental data measured with the growth rate method present a velocity threshold. We show that the threshold value is consistent with the estimate of the free-collision model (FCM), taking into account energy and momentum conservation and the angular dispersion of a quasifree electron within the anion. A general and simple analytical expression for this FCM threshold velocity is presented and tested for the $O^- + N_2$ collision system.

II. EXPERIMENT

The experimental method used here has been described in previous publications [18–20]. The method consists of the application of two different well-established techniques, namely, beam attenuation technique (BAT) and signal growth rate (SGR). Both techniques are used rather than one alone. This offers an improved insight, given that the physics from each technique can be different, as explained ahead. In short, the method is based on measuring the remaining negative ions from an O^- ion beam after their interaction with N_2 gas (BAT), or the resulting neutral atoms of oxygen resulting from the electron loss from the O^- ion-beam interaction with N_2 (SGR). Following, we present a self-standing description of the experimental method with emphasis on the present paper.

In the initial stage, an ion beam of negative oxygen ions is produced. This was carried out by introducing a combination of argon and carbon dioxide gases into a cylindrical chamber made of quartz containing a tungsten filament that was heated to incandescence. The pressure in this chamber was monitored

---

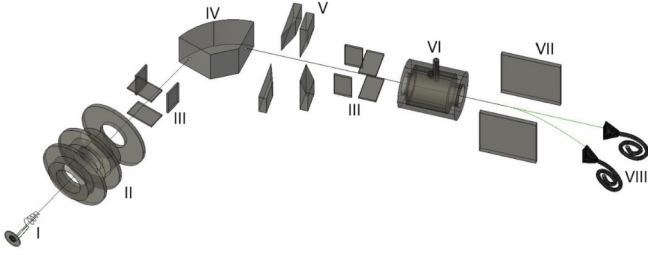*Corresponding author: hinojosa@icf.unam.mx

FIG. 1. Schematic diagram of the apparatus. Not presented to scale. I, filament inside a small quartz chamber (not shown). II, electrostatic lens set. III, steering plates. IV, magnet sector. V, collimating slits. VI, gas cell. VII, analyzing parallel plates (PP). VIII, particle counters or channel electron multipliers (CEMs).

to remain below 25.0 Pa. At one end of the quartz chamber, a metallic cap with a centered 1.5-mm-diameter orifice had a 100-V voltage applied to it in order to accelerate negatively charged particles. Electrons ejected by the filament suffered this acceleration and, in turn, interacted with the gas mixture producing a plasma [10] from which negative ions could be extracted. The assembly containing the chamber was biased to the acceleration voltage. Negative ions from the plasma were expelled through its orifice and in turn repelled or accelerated toward a focusing electrostatic lens set, yielding to a magnetic field where the ions are separated according to their momentum and electric charge, thereby resulting in a monoenergetic, mass-analyzed ion beam. After the magnetic-field region, the ion beam passes through a set of collimating slits to control its width and therefore its intensity. These slits were mounted on linear motion feedthroughs in such a way that the ion beam could be scanned in both directions at right angles on the normal plane to the ion-beam trajectory, and hence be able to monitor its profile too. Before and after the magnetic field's region, two sets of parallel plates (PPs), installed perpendicularly to the ion-beam direction, were used to apply small electric fields to further fine tune the ion-beam trajectory towards a gas cell. The gas cell was built with input and output collimator orifices with diameters of 1.0 and 1.5 mm, respectively, and with a length of 6 cm.

Overall, a single species, monoenergetic, collimated, and focused beam, with a width of ≈ 0.5 mm, enters a gas cell where the interaction of O^- and N_2 occurs in a timeframe of a fraction of 10^{-15} s:

$$O^- + N_2 \longrightarrow O^* + e^- + N_2^* \qquad (1)$$
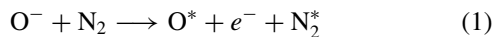
where the star is used to indicate an unknown final internal state. High-purity N_2 gas was used. The resulting neutral oxygen atoms continued in their original trajectory towards a channel electron multiplier (CEM) located in the symmetry axis of the apparatus. The remaining O^- ions from the parent ion beam were separated by a perpendicular electric field set to steer the ions toward a second CEM installed off axis of the accelerator symmetry axis. This electric field was generated with a set of parallel plates (shown in Fig. 1 labeled as PP).

The time of flight of an O^- ion from the output of the ion source to the entrance of the gas cell was of the order of μs. The experiment was performed under high vacuum conditions

so that the mean free path of the ion beam was, at all times, larger than its total trajectory.

To verify if there was a full collection of charged particles, the ion-beam intensity was measured as a function of the PP's electric field. This produced a profile of the ion beam as a function of the PP voltage that systematically showed a distribution with a plateau, thereby showing that the ions were fully collected because their spread was smaller than the width of the CEM's acceptance aperture after dispersion in the gas cell. The CEM's collecting apertures were rectangular with dimensions of 7 mm (width) and 15 mm (height). In addition, as the PPs produce energy analysis, ions that suffer a change of charge do not continue in the direction of the ion beam and, hence, they are not detected.

As a test for the neutral atoms collection, we executed a check performed in another experiment done with the same apparatus and with a lighter H^- ion-beam [20] under similar experimental conditions. In that experiment, the distance between the gas cell and the detectors was changed between two experimental campaigns providing a difference in the aspect ratios (detector's width to distance from the gas cell) of about 18%. This resulted in no measurable difference between the two sets of electron-loss cross sections, thereby verifying that the different amounts of collected neutral atoms were not measurable.

To verify that both CEMs had the same detection efficiencies, the counting rate in the central CEM was measured with the PP electric field set to zero, corresponding to a total count rate of residual neutral atoms plus the O^- parent ion-beam counts. With the PP electric field on, the lateral CEM count rate (parent ion beam) plus the central CEM count rate (residual neutral atoms) was checked to add up to the total count rate in the central CEM. This check was performed under empty gas-cell condition. The CEMs' bias voltage gains were also slightly adjusted for maximum counting rates and the count rates were kept below 1×10^4 s^{-1} as to guarantee optimal performance of the CEMs. These tests were done at each energy.

Systematic errors originate from uncertainties in gas-cell pressure and temperature measurements that propagate a maximum of 11% uncertainty to the cross-section measurements. The relative pressure in the gas cell was monitored with a Baratron capacitance manometer. The kinetic energy had a maximum of 5% uncertainty. In the ion source chamber the base pressure was 8×10^{-4} Pa without gas load, and 5×10^{-2} Pa with gas load. The detection chamber pressure was 5×10^{-5} Pa.

Total electron-loss cross sections were derived from the total count signal measured in each of the CEMs (centered and lateral) as a function of the N_2 gas target thickness (η). Using the signal from the neutral atoms of oxygen (centered CEM) we applied the SGR method, and with the signal in the lateral CEM we applied the BAT.

The target thickness η of the N_2 gas in the gas cell is defined as

$$\eta = \frac{\ell P}{\kappa T}, \qquad (2)$$

where ℓ is its effective length, P is the pressure, and T is the temperature of the gas cell. κ is Boltzmann's constant.
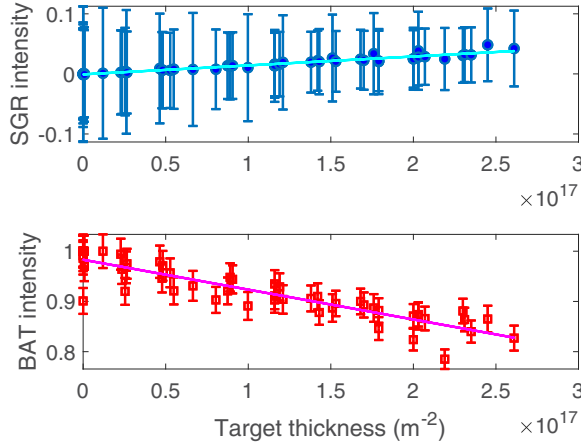
FIG. 2. Examples of the measured data at 5 keV. Top panel corresponds to the reduced data for the SGR method: F_0 as a function of the target thickness η in Eq. (4). The bottom panel corresponds to BAT: I/I_0 as a function of η in Eq. (5).

The SGR method is based on the solutions to the equilibrium equations for the fraction of neutral particles to the number of anions in the ion beam F_0 as a function of the target thickness η. F_0 was derived from

$$F_0 = \frac{I_0 - I_b}{I_i}, \qquad (3)$$

where I_0 is the signal count rate of oxygen atoms that resulted from the interaction with the gas, I_b is the ion-beam background count rate resulting from the ion-beam interaction with the residual vacuum system, and I_i is the count rate corresponding to the initial parent ion beam or the ion-beam intensity with the empty gas cell. The SGR method is described in more detail in Refs. [21–23]. In this method, the fraction F_0 of neutral particles formed after the ion beam loses an electron by collisions with the gas is a function of the initial parent ion-beam intensity and the target thickness. The single-detachment cross section $^s\sigma_{-10}$ was derived from the first-order approximation to F_0:

$$F_0 = {}^s\sigma_{-10}\eta, \qquad (4)$$

where $^s\sigma_{-10}$ is the single collision detachment cross section measured with the SGR method and η is the target thickness.

Examples of a growth rate curve and a beam attenuation curve of the present paper are shown in Fig. 2. All measurements were carried under single collision conditions, i.e., when the functional dependence of the normalized signals to η was linear. Under these conditions, higher-order effects are expected to be negligible.

The BAT consists of measuring the decline of the parent ion-beam intensity as a function of the gas thickness η. The cross section was derived from

$$I = I_i \exp\left(-^b\sigma_{-10}\eta\right), \qquad (5)$$

where η is given by Eq. (2), I is the ion-beam intensity as a function of η, and I_i is the initial intensity of the ion beam. $^b\sigma_{-10}$ is the total electron-detachment cross section. An example of a BAT curve for the present data is shown in Fig. 2. The
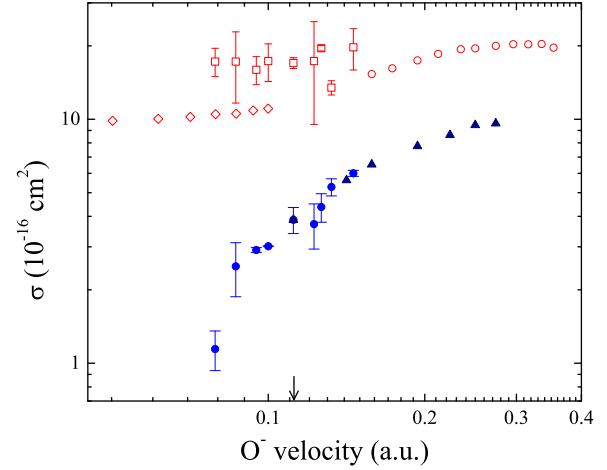

FIG. 3. Total electron-loss cross sections for Eq. (1) as a function of the speed in atomic units. Data measured with BAT (present paper): open squares. Diamonds: Bennet *et al.* [27]. Open circles: Tsuji *et al.* [28]; the sum of $\sigma_{-10} + \sigma_{-11}$ is plotted to account for the total electron loss. Data measured with SGR (present paper): closed circles. Up triangles: Matić and Čović [26]. Error bars for the present data correspond to total errors, standard deviation, and systematic uncertainties. Errors for cited works are not plotted. The arrow indicates the velocity corresponding to 5 keV.

BAT technique has been used and described in more detail in Refs. [24,25].

The dispersion of the data in Fig. 2 is mainly caused by the instability in the ion-beam intensity, originated by plasma fluctuations in the ion source. In the case of BAT, the vertical axes of Fig. 2 correspond to the ion-beam intensity readings normalized to I_i. In the case of SGR, the vertical axis corresponds to the average of the initial and final I_i ion-beam currents. This establishes a source of systematic uncertainty that is different for each method and could explain, at least in part, the difference in the dispersion of both sets of data. Data sets where the ion-beam intensity differed by 10% or more during the beginning and the ending of an experimental measurement were discarded.

Once a distribution of cross-section values was obtained at each energy, standard deviations were derived as a measure of the statistical errors, that were in turn combined with the systematic uncertainty to derive total errors per energy point. Our whole set of data was normalized by a single constant factor so that our cross-section data point measured at 5 keV using SGR coincides with the 5-keV correspondent value also measured using SGR by Matić and Čović [26].

III. RESULTS AND DISCUSSION

The present data are shown in Fig. 3. Data points correspond to the BAT (open data points) and to the SGR (closed data points). In the figure are also plotted data from Bennet *et al.* [27], and Tsuji *et al.* [28] measured with BAT, and data from Matić and Čobić [26], measured with SGR. In Fig. 3 we note that there is a discrepancy between the data measured with BAT versus the data measured with SGR. The present data also reproduce a similar situation.

At first approximation, BAT and SGR cross sections are expected to have similar values, given that the ion-beam composition is only of O^- ions and that the dependence of the signals with target density is under single collision conditions. However, the cross sections measured with the two techniques are very different. This kind of disagreement at the low-energy interval has been a question in the research field and is not restricted to the $O^- + N_2$ collision system [29].

It is important to note that by using BAT the total decrease of the O^- ions from the ion beam is measured, therefore all processes that may cause a reduction of the ion-beam intensity are accounted for. By using SGR method, only neutral atoms resulting from the interaction with N_2 are detected, which means that processes that produce neutral atoms in the direction of the ion beam are accounted for.

This difference may be caused by a process that is not measured in the SGR method and influences mainly the BAT cross section for $^b\sigma_{-10}$ to be larger than $^s\sigma_{-10}$. Other processes involved in the interaction may be direct electronic detachment, electron transfer (ET), double detachment (DD), and single detachment followed by electron transfer where the final state is O^0. However, the last process would imply secondary collisions and can be ruled out from single collision conditions (see Fig. 2).

In the case of the DD channel, its contribution has been measured to be negligible for other collision systems [30,31], and for $O^- + N_2$, in particular, [26]. In this experiment, we measured the relative contribution of the resulting O^+ yield by reversing the polarity of the PP showing a very low counting rate of, at most, one order of magnitude lower when compared to the intensity of the SGR signal. This demonstrates that the DD channel contribution cannot justify the difference. In the case of ET, this process cannot be separated by these methods and its contribution is expected to have the same effect in both techniques.

Another possibility is electric-field-induced detachment. This possibility is discarded on the next basis: a procedure in this experiment consisted in verifying the detectors to have similar efficiencies. This was carried out by measuring the count rates with the electric field on and off, and without gas load in the gas cell. This shows that the electric field alone did not induce measurable electron detachment. The PP electric-field intensity demonstrated not to induce electron detachment at all energies according to this test. In terms of the electric-field intensity ($<300 \, \mathrm{V\,cm^{-1}}$) and for the ground state of O^-, the electric field is not expected to induce electron detachment [32].

Figure 3 shows that the present BAT data are consistent with data from Bennet *et al.* [27] and Tsuji *et al.* [28], measured with the same method. For the case of the cross sections measured with the SGR method, the present data agree with the general tendency of the results from Matić and Čović [26] to which the present data have been normalized to using their 5-keV point (see in Fig. 3 the arrow indicating the point of the velocity scale corresponding to 5 keV).

A possible explanation for the difference between both methods is the presence of autodetaching states. In previous studies, we have derived lifetimes for the autodetaching states [19,20] possibly formed during the interaction with the gas target. However, lifetime studies for this kind of state are
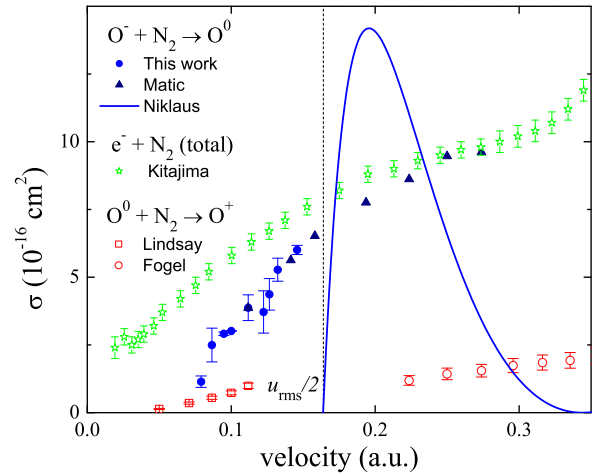

FIG. 4. Cross sections as a function of the speed in atomic units, for processes relevant to the free-electron-model hypothesis for the present interaction system. Open stars: electron-scattering cross sections $e^- + N_2$ of Kitajima [33]. Electron-detachment cross sections for neutral projectiles $O^0 + N_2$: open squares, Lindsay [34]; open circles, Fogel [35]. Electron-detachment cross sections for anionic projectiles $O^- + N_2$: closed up triangles, Matić and Čović [26]; closed circles, present SGR data; line, Eq. (6). Vertical dotted line: O^- velocity given by Eq. (10).

scarce, and further experimental and theoretical studies are needed to quantify the relevance of these autodetaching states.

Although the present BAT cross sections reproduce the general tendency, they do not agree with previously reported values. This is congruent with the hypothesis of autodetaching metastable states because the cross-section values would depend on the time of flight within the machine.

In Fig. 4 we compare data for $O^- + N_2$ single-electron-detachment cross sections measured by SGR method and cross sections for two related projectiles incident on N_2: electrons and atomic oxygen. The total electron scattering cross sections for $e^- + N_2$ agree with the data for $O^- + N_2$ at $v \approx 0.25$ a.u., showing that above this velocity the description of the anion as a quasifree electron plus a neutral core is meaningful for the $O^- + N_2$ detachment collision channel. The comparison between $O^- + N_2$ and $O^0 + N_2$ electron-detachment cross sections also supports the quasifree-electron picture. Using a simplified electron-plus-core model for the O^- projectile, collisions involving the atomic oxygen projectile, O^0, can be used to estimate the contribution of core electrons of O^- to the total detachment cross sections. The $O^0 + N_2$ cross sections are much smaller than the $O^- + N_2$ ones. Thus, the detachment cross section for the $O^- + N_2$ system is dominated by the contribution from the O^- loosely bound electron.

In order to estimate projectile-electron-loss cross sections, Bohr and Lindhard [36,37] calculated the cross section for energy transfer greater than T in a collision between a free electron at rest (in the projectile's frame of reference) and a heavy particle (the target) with charge Z_{EF}, where $T_{\max} = 2mv^2$ is the upper limit for energy transfer in such a collision. Thus, in this approach, the neutral target is modeled as a dressed charge that ionizes the electron loosely

bound to the projectile. Niklaus *et al.* [38,39] include in the Bohr-Lindhard (B-L) version of the FCM an empirical velocity-dependent effective charge $Z_{EF}(v)$ and obtain

$$\sigma(v) = \begin{cases} 0, & \text{if } v < v_0 \\ \sigma_0(v)\left[1 - \left(\frac{v_0}{v}\right)^2\right], & \text{if } v > v_0 \end{cases} \quad (6)$$

with

$$v_0 = \frac{u_{rms}}{2}, \quad (7)$$

$$\sigma_0(v) = \pi a_B^2 Z_{EF}(v)^2 \left(\frac{1}{v v_0}\right)^2, \quad (8)$$

and

$$Z_{EF}(v) = Z_T \left\{ 1 - 1.08 \exp\left[-80.1 Z_T^{-0.506}(v/c)^{0.996}\right]\right\}, \quad (9)$$

where a_B is the Bohr radius, c is the velocity of light, and Z_T is the target atomic number. For anions, the Bohr-Lindhard threshold velocity is parametrized in terms of the electron affinity (EA) [40,41] as

$$v_0 = \frac{1}{2}\sqrt{\frac{EA\ [eV]}{13.6}}. \quad (10)$$

In Fig. 4 we also show the results from Eq. (6) for $O^- + N_2$. The agreement with experimental data is poor, for two reasons.

(i) The modeling of the target as a dressed charged particle is a naive approximation to a much more complex problem [42], and is especially inadequate for collision between an electron and the N_2 target [17].

(ii) The value for the free-collision threshold is overestimated due to neglecting the velocity of the ionized electron within the projectile frame of reference.

Variations of the FCM deal with these limitations by including a combination of previously known cross sections for electron-impact elastic scattering by the target and the projectile electronic-velocity distribution (e.g., Refs. [43–46]).

This more general FCM approach includes a velocity threshold for the electron detachment since there is still a maximum momentum that the massive target can transfer to the projectile's electron. This limit is now affected by the angular dependence of elastic scattering of a free electron by the target and by the electronic distribution of the anionic projectile [46–48]. The FCM calculations can, in principle, determine detachment cross sections combining contributions from projectile electrons with different momenta.

However, quadruple integrals involved in this approach are a practical limitation to FCM calculations of cross sections involving anionic projectiles and molecular targets. Thus, FCM calculations are often restricted to the intermediate-to-high velocity regime (e.g., Refs. [24,25,46–51]). In the present paper, we combine the Bohr-Lindhard approach with a threshold analysis of the general Risselman approach in order to obtain a simple analytical expression of the FCM threshold behavior that takes into account the electronic velocity distribution within the projectile.

In Risselmann formulation of the FCM [46], the total-electron-loss cross section $Q(v_N)$ for a one-electron projectile

for which the nucleus has a velocity $\mathbf{v}_N = v_N \hat{z}$ is given by

$$\int_0^\infty f(u)du \int_0^\pi \frac{1}{2}\sin(\beta)d\beta \int_0^{2\pi} d\phi \int \sigma(v,\theta)\sin(\theta)d\theta, \quad (11)$$

where u and β are, respectively, the modulus and the polar angle of the projectile electron in the projectile frame of reference, and v is the velocity of the electron in the laboratory frame of reference. $f(u)$ is the distribution of absolute values of the velocity of the projectile's electron. $\sigma(v,\theta)$ is the differential electron-scattering cross section at an angle θ for a free electron impinging on the target. For elastic collisions, $\Delta E = 0$, Risselmann's expression of the inequality regarding energy and momentum conservation reduces to

$$[v_N + u\cos(\beta)][1 - \cos(\theta)] + u\sin(\beta)\cos(\phi)\sin(\theta)$$
$$\geqslant u_{rms}^2/(2v_N), \quad (12)$$

where the characteristic anion velocity u_{rms} (the root-mean-square velocity) is obtained from $EA = mu_{rms}^2/2$. While u_{rms} is often interpreted as a root-mean-squared value, it is normally obtained from experimental EA values [46–48]. Near threshold, close collisions are most relevant to higher momentum transfer. Thus, we approximate $\theta \approx \pi$ and, using $v_0 = u_{rms}/2$, obtain from Eq. (12)

$$\frac{v_N}{v_0}\left(\frac{v_N}{v_0} + \frac{u}{v_0}\cos(\beta)\right) \geqslant 1. \quad (13)$$

If the electron velocity in the projectile frame of reference (u) is negligible compared to the anion nucleus velocity, then $v_N \geqslant v_0$ and v_0 is the threshold velocity (as in the Bohr-Lindhard approach). Otherwise, Eq. (13) results in a modified threshold velocity that is a function of the product $u\cos(\beta)$, which is the z component of the electron velocity within the anion, u_z. Defining $s = v_N/v_0$ and $t = u/v_0$, we can write

$$t\cos(\beta) \geqslant \left(\frac{1}{s} - s\right). \quad (14)$$

The particular case $\cos(\beta) = \pm 1$ gives electron momentum parallel or antiparallel to the anion's nucleus velocity, resulting in the s positive limit solutions

$$s_< = \sqrt{1 + \left(\frac{t}{2}\right)^2} - \frac{t}{2}, \quad (15)$$

$$s_> = \sqrt{1 + \left(\frac{t}{2}\right)^2} + \frac{t}{2}. \quad (16)$$

If the distribution $f(u) = \delta(u - u_{rms})$ then $t = 2$, and therefore $s_< = \sqrt{2} - 1$ and $s_> = \sqrt{2} + 1$. Thus, within the δ approximation for $f(u)$, the modified threshold nucleus velocity (denoted by $v_<$) is $v_0 s_<$, i.e.,

$$v_< = (\sqrt{2} - 1)v_0 \approx 0.414 \frac{1}{2}\sqrt{\frac{EA\ [eV]}{13.6}}. \quad (17)$$

The ratio R between the cross section for projectile electron loss σ_{O^-} and total electron elastic cross sections σ_e can be used to compare experimental data to the FCM results. Within the Bohr-Lindhard approach, assuming $\sigma_0 = \sigma_e$, this leads to an
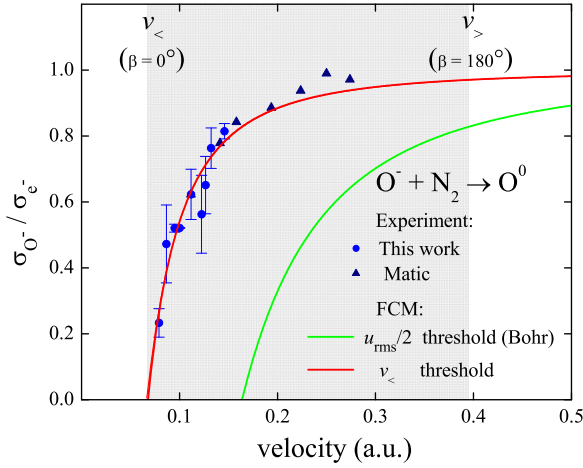
FIG. 5. Ratio of cross sections for $O^- + N_2$ as a function of the speed in atomic units for projectile electron loss and total electron scattering by N_2 (using $e^- + N_2$ of Kitajima [33]). Closed circles, present SGR data; closed up triangles, Matić and Čobić [26]; blue line, Bohr-Lindhard FCM; red line, modification of Bohr-Lindhard FCM with the $v_<$ velocity threshold; the gray shaded area highlights the velocity range with threshold affected (within the FCM) by the angle β between the incidence direction and projectile electron direction. The region is delimited by $v_<$ ($\beta = 0$) and $v_>$ ($\beta = 180°$).

expression unaffected by the dressed-charge approximation to the target:

$$R_{\text{B-L}} = 1 - \left(\frac{v_0}{v}\right)^2. \tag{18}$$

We substitute the Bohr-Lindhard threshold velocity by $v_<$ [Eq. (17)] and obtain

$$R = 1 - \left(\frac{(\sqrt{2}-1)\,v_0}{v}\right)^2. \tag{19}$$

Figure 5 shows ratios of $O^- + N_2$ projectile electron loss to the $e^- + N_2$ total electron elastic cross sections of Kitajima *et al.* [33]. For sufficiently high velocities, the FCM predicts a ratio of 1. The ratios for the higher-energy data of Matić and Čović [26], with velocities in the range between v_0 and u_{rms}, are close to 1.

We show in Fig. 5 the FCM results obtained from the B-L approach [Eq. (18)] and the B-L result with threshold velocity v_0 replaced by the $v_<$ expression obtained in the present paper [Eq. (19)]. We represent the range of velocities with β integration restrictions [Eq. (14)] by the gray shaded area. The comparison between the two FCM results and the experimental data, both from this paper and from Matić and Čobić [26], shows that the substitution of the threshold velocity v_0 by $v_<$ results in good FCM description of the anionic-projectile collision system studied in the present paper. It also suggests that for anionic projectiles (for which the EA values are at most of a few eV), even close to the FCM threshold, the β distribution is more relevant to cross-section convolution than the distribution of absolute values u [see Eq. (11)]. The parametrization of R only on EA, via $v_<$, provides a contribution in the pursuit of scaling laws common to few-keV

projectile-electron-loss cross sections for anionic projectiles (e.g., Refs. [11,13–16]).

It is important to note that the existence of the threshold for quasifree electron detachment does not imply that the projectile-electron-detachment cross section is expected to be zero below threshold. At very low velocities, molecular states formed by projectile and target can result in large cross sections [52]. In the case of $O^- + N_2$ those states are related to the temporary formation of a N_2O^- complex [53]. The velocity dependence of projectile-electron-detachment cross sections with a peak before threshold was observed, for example, in $O_2^- + N_2$ collisions [54].

IV. CONCLUSIONS

The total projectile-electron-loss cross sections for $O^- + N_2$ in the energy range from 2.5 to 8.5 keV have been measured with two methods: the beam attenuation ($^b\sigma_{-10}$) and the signal growth rate techniques ($^s\sigma_{-10}$). Close to this energy range, previously published cross sections show a long-standing considerable disagreement, depending on the measurement method used. The present data have also shown this discrepancy between results originating by the two methods. At the same time, for both methods, the present results are consistent with the cross sections measured with corresponding techniques, and further experimental and theoretical studies are needed to address this difference.

From a fundamental point of view, a negative ion can be considered a simple carrier to a free electron under certain circumstances. The FCM is based on this assumption. However, the validity of this model close to the velocity threshold has been rarely assessed. In this paper, we present a general, simple, and analytical expression for the velocity threshold within the FCM, easily applicable for anionic projectiles. When applied to the $O^- + N_2$ collision system, the expression shows consistency with the experimental threshold value obtained from the velocity dependence of our data.

In addition to its fundamental interest, negative ions are of relevance in plasma modeling because electron loss from negative ions can modify the electron density function. In this paper, we demonstrate that the process of electron loss from O^- at a speed v above ≈ 0.25 a.u. for the cross section for electron detachment is as relevant as electron scattering, and in a given plasma environment with a high density of negative ions, such as carbohydrate plasma, electron detachment could be even more relevant than electron scattering.

[1] A. Ramírez-Solís, J. Vigué, G. Hinojosa, and H. Saint-Martin, Solving the CH_4^- riddle: The fundamental role of spin to explain metastable anionic methane, Phys. Rev. Lett. **124**, 056001 (2020).

[2] M. J. Jensen, U. V. Pedersen, and L. H. Andersen, Stability of the ground state vinylidene anion H_2CC^-, Phys. Rev. Lett. **84**, 1128 (2000).

[3] Yu. V. Medvedev, Acceleration and trapping of ions upon collision of ion-acoustic solitary waves in plasma with negative ions, Plasma Phys. Rep. **45**, 230 (2019).

[4] A. Mondal, S. V. Rahul, R. Gopal, D. Rajak, M. Anand, J. Jha, S. Tata, A. K. Dharmadhikari, A. K. Gupta, and M. Krishnamurthy, Misjudging negative ions for electrons in intense laser plasma diagnostics, AIP Adv. **9**, 025115 (2019).

[5] A. J. Coates, F. J. Crary, G. R. Lewis, D. T. Young, J. H. Waite, Jr., and E. C. Sittler, Jr., Discovery of heavy negative ions in Titan's ionosphere, Geophys. Res. Lett. **34**, L22103 (2007).

[6] M. A. Cordiner and S. B. Charnley, Negative ion chemistry in the coma of comet 1P/Halley, Meteorit. Planet. Sci. **49**, 21 (2014).

[7] L. B. Strogonova, A. E. Sorokin, Y. A. Vasin, and A. E. Belyavskii, Creating an atmosphere within spacecraft, Russ. Engin. Res. **39**, 813 (2019).

[8] R. C. Fortenberry, Interstellar anions: The role of quantum chemistry, J. Phys. Chem. A **119**, 9941 (2015).

[9] M. Khamesian, N. Douguet, S. F. dos Santos, O. Dulieu, M. Raoult, W. J. Brigg, and V. Kokoouline, Formation of CN^-, C_3N^-, and C_5N^- molecules by radiative electron attachment and their destruction by photodetachment, Phys. Rev. Lett. **117**, 123001 (2016).

[10] E. M. Hernández, L. Hernández, C. Martínez-Flores, N. Trujillo, M. Salazar, A. Chavez, and G. Hinojosa, Electron detachment cross sections of CH_4^- colliding with O_2 and N_2 below 10 keV energies, Plasma Sources Sci. Technol. **23**, 015018 (2014).

[11] F. Zappa, G. Jalbert, L. F. S. Coelho, A. B. Rocha, S. D. Magalhães, and N. V. de Castro Faria, Absolute electron detachment cross sections of atomic anions of the second and third periods incident on noble gases, Phys. Rev. A **69**, 012703 (2004).

[12] A. C. F. Santos and R. D. DuBois, Scaling laws for single and multiple electron loss from projectiles in collisions with a many-electron target, Phys. Rev. A **69**, 042709 (2004).

[13] S. Wu, X. Zhanga, and G. Li, Single-electron detachment cross sections for negative ions of transition elements colliding with gases, At. Data Nucl. Data Tables **93**, 575 (2007).

[14] Z. Geng, X. Bai, B. Wei, and X. Zhang, Single-electron detachment cross sections of Co^- and Ir^- in collision with Ar and an empirical formula for single-electron detachment cross sections of negative ions in collision with Ar, Can. J. Phys. **91**, 175 (2013).

[15] G. Min, G. Guo, D. Wang, and X. Zhang, Single-electron-detachment cross sections of Fe^-, Ru^-, Ni^-, Pd^- and Pt^-, in collisions with inert-gas atoms, Phys. Rev. A **95**, 062706 (2017).

[16] Y. Yang, J. Wang, Y. Tian, and X. Zhang, Single and double electron detachment absolute cross sections of H^- and D^- in collisions with SF_6 and CF_4, Can. J. Phys. **100**, 272 (2022).

[17] M.-Y. Song, H. Cho, G. P. Karwasz, V. Kokoouline, and J. Tennyson, Electron scattering on molecular nitrogen: Common gas, uncommon cross sections, Eur. Phys. J. D **77**, 105 (2023).

[18] E. M. Hernández and G. Hinojosa, Collision induced electron detachment cross sections of the H_2CC^- anion below 10 keV on O_2 and N_2, Int. J. Mass Spectrom. **424**, 35 (2018).

[19] A. Lira, A. A. Martínez, A. Escalante, S. Vergara, and G. Hinojosa, Electron loss of CH^- and CH_2^- induced by interactions with N_2 and O_2 at keV energies, Int. J. Mass Spectrom. **469**, 116681 (2021).

[20] S. Vergara, A. A. Martínez, F. R. Peñalver, and G. Hinojosa, Electron detachment cross section of H^- induced by collisions with O_2, J. Phys. B **54**, 155201 (2021).

[21] M. H. Salazar-Zepeda, C. Gleason, E. González, O. González-Magaña, and G. Hinojosa, Double electron capture by protons in collisions with H_2, Nucl. Instrum. Meth. B **268**, 1558 (2010).

[22] J. S. Allen, X. D. Fang, A. Sen, R. Matulioniene, and T. J. Kvale, Double-electron detachment cross sections in intermediate-energy H^- plus noble-gas collisions, Phys. Rev. A **52**, 357 (1995).

[23] E. W. McDaniel, J. B. A. Mitchell, and M. E. Rudd, *Atomic Collisions, Heavy Particle Projectiles* (Wiley, New York, 1993).

[24] R. F. Nascimento, S. L. A. Mello, B. F. Magnani, M. M. Sant'Anna, G. Jalbert, and N. V. de Castro Faria, Total detachment cross sections of C^-, CH^-, C_2^-, and C_2H^- incident on N_2 at keV energies, Phys. Rev. A **87**, 062704 (2013).

[25] G. Jalbert, R. F. Nascimento, C. R. de Carvalho, Carla R. Carvalho, B. F. Magnani, A. C. F Santos, A. B. Rocha, M. M. Sant'Anna, and N. V. de Castro Faria, Electron-detachment cross section for CN^- and O_2^- incident on N_2 at intermediate velocities, Phys. Rev. A **89**, 012712 (2014).

[26] M. Matić and B. Čobić, Electron loss by C^- and O^- ions in gaseous targets, J. Phys. B **4**, 111 (1971).

[27] R. A. Bennett, J. T. Moseley, and J. R. Peterson, Electron loss cross sections for O^-, O_2^-, NO_2^-, and NO_3^- in several gases, J. Chem. Phys. **62**, 2223 (1975).

[28] H. Tsuji, J. Ishikawa, T. Maekawa, and T. Takagi, Electron detachment cross-sections for heavy negative-ion beam, Nucl. Instrum. Meth. B **37-38**, 231 (1989).

[29] F. Rahman and B. Hird, Electron detachment atomic cross sections from negative ions, At. Data Nucl. Data Tables **35**, 123 (1986).

[30] E. M. Hernández, L. Hernández, L. N. Serkovic-Loli, and G. Hinojosa, Collisional induced double electron loss of NO^- and CH_4^- anions below 10 keV energies, Int. J. Mass Spectrom. **403**, 39 (2016).

[31] J. Ishikawa, H. Tsuji, and T. Maekawa, Electron detachment cross-sections in low energy heavy negative ion beam apparatus, Vacuum **39**, 1127 (1989).

[32] M. Halka, P. G. Harris, A. H. Mohagheghi, R. A. Reeder, C. Y. Tang, H. C. Bryant, J. B. Donahue, and C. R. Quick, Electric-field effects on H^- photodetachment partial cross sections above 13.4 eV, Phys. Rev. A **48**, 419 (1993).

[33] M. Kitajima *et al.*, Low-energy and very-low energy total cross sections for electron collisions with N_2, Eur. Phys. J. D **71**, 139 (2017).

[34] B. G. Lindsay, W. S. Yu, K. F. McDonald, and R. F. Stebbings, Electron capture and loss by kilo-electron-volt oxygen atoms in collisions with He, H_2, N_2, and O_2, Phys. Rev. A **70**, 042701 (2004).

[35] I. M. Fogel, V. A. Ankudinov, and D. V. Pilipenko, Electron capture and loss in collisions of fast carbon and oxygen atoms with gas molecules, Sov. Phys. JETP **8**, 601 (1959).

[36] N. Bohr, The penetration of atomic particles through matter, Dan. Vidensk. Selsk. Mat.-Fys. Medd. **18**, 1 (1948).

[37] N. Bohr and K. Lindhard, Electron capture and loss by heavy ions penetrating through matter, Dan. Vidensk. Selsk. Mat.-Fys. Medd. **28**, 1 (1954).

[38] Th. R. Niklaus, G. Bonani, Z. Guo, M. Suter, and H.-A. Synal, Optimising tandem accelerator stripping efficiency by simulation of charge changing processes, Nucl. Instrum. Meth. B **92**, 115 (1994).

[39] R. O. Sayer, Semi-empirical formulas for heavy-ion stripping data, Rev. Phys. Appl. (Paris) **12**, 1543 (1977).

[40] M. K. Kristiansson, K. Chartkunchand, G. Eklund, O. M. Hole, E. K. Anderson, N. de Ruette, M. Kaminska, N. Punnakayathil, J. E. Navarro-Navarrete, S. Sigurdsson, J. Grumer, A. Simonsson, M. Björkhage, S. Rosén, P. Reinhed, M. Blom, A. Källberg, J. D. Alexander, H. Cederquist, H. Zettergren, H. T. von Schmidt, and D. Hanstorp, High-precision electron affinity of oxygen, Nat. Commun. **13**, 5906 (2022).

[41] C. Ning and Y. Lu, Electron affinities of atoms and structures of atomic negative ions, J. Phys. Chem. Ref. Data **51**, 021502 (2022).

[42] E. C. Montenegro, W. E. Meyerhof, and J. H. McGuire, Role of two-center electron-electron interaction in projectile electron excitation and loss, *Advances in Atomic and Molecular Optical Physics Vol. 34* (Academic Press, New York, 1994), pp. 249–300.

[43] D. R. Bates and J. C. G. Walker, Quenching of auroral hydrogen line emission by collisional ionization, Planet. Space Sci. **14**, 1367 (1966).

[44] D. R. Bates and J. C. G. Walker, A classical impulse approximation treatment of collisional detachment from H⁻ ions, Proc. Phys. Soc. **90**, 333 (1967).

[45] D. R. Bates, V. Dose, and N. A. Young, Classical treatment of electron loss, J. Phys. B **2**, 930 (1969).

[46] K. Riesselmann, L. W. Anderson, L. Durand, and C. J. Anderson, Classical impulse approximation for the electron loss from H(1s) or H⁻ projectiles passing through various gas targets, Phys. Rev. A **43**, 5934 (1991).

[47] G. M. Sigaud, Free-collision model calculations for the electron detachment of anions by noble gases, J. Phys. B **41**, 015205 (2008).

[48] G. M. Sigaud, Free-collision model calculations for projectile electron loss by the H_2 molecule, J. Phys. B **44**, 225201 (2011).

[49] J. Heinemeier, P. Hvelplund, and F. R. Simpson, Collisional detachment cross sections for H⁻ and He⁻ at high energies, J. Phys. B **9**, 2669 (1976).

[50] M. M. Sant'Anna, F. Zappa, A. C. F. Santos, A. L. F. de Barros, W. Wolff, L. F. S. Coelho, and N. V. de Castro Faria, Electron-detachment cross sections of halogen negative-ion projectiles for inertial confinement fusion, Plasma Phys. Control. Fusion **46**, 1009 (2004).

[51] M. M. Sant'Anna, F. Zappa, G. Jalbert, A. C. F. Santos, B. F. Magnani, L. F. S. Coelho, and N. V. de Castro Faria, Electron-loss cross sections for heavy-ion beam probe using gold beams: Experiment and theory, Plasma Phys. Control. Fusion **51**, 045007 (2009).

[52] V. A. Esaulov, Electron detachment from atomic negative ions, Ann. Phys. Fr. **11**, 493 (1986).

[53] J. Comer and G. J. Schulz, Measurements of electron-detachment cross sections from O⁻ and S⁻, Phys. Rev. A **10**, 2100 (1974).

[54] M. Mendes, C. Guerra, A. I. Lozano, D. Rojo, J. C. Oller, P. Limão-Vieira, and G. García, Experimental electron-detachment cross sections for collisions of O_2^- with N_2 molecules in the energy range 50–7000 eV, Phys. Rev. A **99**, 062709 (2019).